THE MAGNITUDE DISTRIBUTION OF DYNAMICALLY TRIGGERED EARTHQUAKES

A thesis submitted in partial satisfaction
of the requirements for the degree of

MASTER OF SCIENCE

in

EARTH SCIENCES

by

Stephen Hernandez

March 2014

The Thesis of Stephen Hernandez
is approved:

Professor Emily E. Brodsky, Chair

Professor Susan Y. Schwartz

Professor Thorne Lay

Tyrus Miller
Vice Provost and Dean of Graduate Studies

Table of Contents	**Page**

List of Figures	**Page**

The magnitudes of dynamically triggered earthquakes

by

Stephen Hernandez

Abstract Large dynamic strains carried by seismic waves are known to trigger seismicity far from their source region. It is unknown, however, whether surface waves trigger only small earthquakes, or whether they can also trigger large, societally significant earthquakes. To address this question, we use a mixing model approach in which total seismicity is decomposed into 2 broad subclasses: "triggered" events initiated or advanced by far-field dynamic strains, and "untriggered" spontaneous events consisting of everything else. The *b*-value of a mixed data set, b_{MIX}, is decomposed into a weighted sum of *b*-values of its constituent components, b_T and b_U. For populations of earthquakes subjected to dynamic strain, the fraction of earthquakes that are likely triggered, f_T, is estimated via inter-event time ratios and used to invert for b_T. The confidence bounds on b_T are estimated by multiple inversions of bootstrap resamplings of b_{MIX} and f_T. For Californian seismicity, data are consistent with a single-parameter Gutenberg-Richter hypothesis governing the magnitudes of both triggered and untriggered earthquakes. Triggered earthquakes therefore seem just as likely to be societally significant as any other population of earthquakes.

Acknowledgments

I would like to thank Emily Brodsky and Nicholas van der Elst for their guidance and extensive conversations that made this thesis possible.

The magnitudes of dynamically triggered earthquakes

by

Stephen Hernandez

Transient strains delivered by large amplitude seismic waves are frequently associated with seismicity rate increases in the far-field at both active margins and stable plate interiors [*Hill et. al.*, 1993; *Velasco et. al.*, 2008]. This triggering phenomenon is frequently attributed to dynamic stresses since static stresses decay quickly at such large distances (≥2-3 fault lengths) [*King et. al.*, 1994]. One of several outstanding problems associated with remote dynamic triggering is whether the magnitudes of triggered earthquakes are significantly different from the magnitudes of ambient seismicity. For instance, *Parsons and Velasco* [2011] investigated whether large (M≥7) events are capable of dynamically triggering other large (5≤M≤7) earthquakes in the far-field, and found that they were unable to observe near-instantaneous triggering of large events in the far-field. This conclusion was somewhat upended by the 2012 Sumatra-East Indian Ocean earthquake, which triggered a clear increase in magnitude 5+ earthquakes over several days [*Pollitz et al.,* 2012]. Statistical interpretations of seismicity suggest that even when the initial triggered earthquakes are small, a cascade of events drawn from a single magnitude distribution can culminate in large, societally significant earthquakes [*Ogata, 1988; Felzer et. al.*, 2002; *Felzer et. al.*, 2004]. With this prospect in mind, we seek to determine if populations of earthquakes that include many remotely triggered events have a different mean magnitude than those that contain very few triggered earthquakes.

This article begins with an overview of earthquake frequency-magnitude distributions, followed by a discussion of a mixing model that relates the observable *b*-value of a mixed group of triggered and untriggered earthquakes, b_{MIX}, to the parameter of interest (the *b*-value of the triggered events, b_T). Utilizing this model requires constructing populations of earthquakes with an inferred fraction of triggered events. We proceed to form groups of earthquakes that have been affected by dynamic strains of similar amplitude. We measure the fraction of triggered events in each of these groups using an inter-event time statistic and invert for b_T.

Earthquake Magnitude Distributions

The magnitude-frequency distribution of earthquakes over broad swaths of regions and time can be represented by the cumulative Gutenberg-Richter (GR) distribution

$$\log_{10}(N(m)) = a - b \cdot m \tag{1}$$

where *a* and *b* are constants, *N(m)* is the number of earthquakes with magnitude greater than *m*, and $m \geq M_C$, with M_C the magnitude of completeness of the catalog [*Ishimoto and Iida*, 1939; *Gutenberg and Richter*, 1942]. The Aki-Utsu maximum likelihood estimator for the parameter *b* is

$$b = \frac{\log_{10}(e)}{\langle M \rangle - M_C} \tag{2}$$

where $\langle M \rangle$ is the mean magnitude [*Aki*, 1965; *Utsu*, 1965].

The Gutenberg-Richter distribution is a representation of the exceedance probabilities for a given range of magnitudes. For constant *a*-value, differences in *b*-value represent differences in the relative hazard of large earthquakes in different regions. Characterizing and identifying differences in *b*-values has implications for both hazard analysis and the physical mechanisms of earthquake nucleation [*Frohlich and Davis*, 1993; *Utsu*, 1999; *Schorlemmer et. al.*, 2005]. Other parameterizations of the frequency-magnitude distribution are possible, including a truncated distribution that includes maximum magnitude as a free parameter [*Holschneider et al.*, 2011]. However, resolving a multivariate distribution requires even more data than resolving differences in mean magnitude. As will be shown below, resolving even mean magnitude differences is at the limit of the current data resolution and so no more complex model is warranted by the data.

Mixing Model

Suppose a sequence of earthquake magnitudes, M_i^{mix}, exists such that it is composed entirely of either triggered, M_j^T, or untriggered, M_k^U, events. The sum of magnitudes of the mixed (composite) catalog can be expressed as

$$\sum_{i}^{n_{tot}} M_i^{mix} = \sum_{j}^{n_T} M_j^T + \sum_{k}^{n_U} M_k^U \tag{3}$$

where n_T and n_U are the total number of triggered and untriggered observations, and $n_{tot} = n_T + n_U$. Equation (3) can be recast as a weighted sum of the means of the individual components

$$\langle M_{mix} \rangle = f_T \cdot \langle M_T \rangle + (1 - f_T) \cdot \langle M_U \rangle \tag{4}$$

where $f_T = n_T/n_{tot}$. Finally, since the Aki-Utsu equation (equation (2)) relates the *b*-value of a given dataset to the mean magnitude of that dataset, it is trivial to show that

$$b_T = \frac{f_T \cdot b_U}{\frac{b_U}{b_{MIX}} + f_T - 1} \tag{5}$$

In this formulation, we are assuming that the minimum magnitude of completeness is equivalent for both subcatalogs, M_T and M_U. Application of a maximum likelihood methodology yields similar results [*Kijko and Smit, 2012; Appendix A*]. In practice, we impose 2 regularity conditions to stabilize the inversion and to produce physically meaningful results: the denominator in equation (5) must be greater than 0 and f_T must be greater than 0 (*i.e.,* n_T greater than 0). For f_T greater than 0, the denominator is greater than 0 if $b_U/b_{MIX} > 1 - f_T$.

To use equation (5), we need to construct populations of earthquakes with differing fractions triggered and then perform two distinct tasks: (1) measure b_{MIX} in the combined population and (2) determine the fraction of triggered events. Additionally, we

need to find a group of earthquakes with a very low fraction of triggering in order to estimate the untriggered *b*-value b_U.

We will accomplish all of these goals by capitalizing on the previous observation that the fraction of triggered events in the far-field is a well-defined function of the peak amplitude of the seismic waves, *i.e.*, larger amplitude waves trigger more events [*van der Elst and Brodsky*, 2010]. Therefore, we can construct groups of earthquakes that immediately follow dynamic strains from distant earthquakes. The groups of earthquakes following large amplitude shaking will have a large (and measurable) triggered fraction, f_T, and can be used in conjunction with equation (5) to measure the *b*-value of triggered earthquakes, b_T. Those following small or extremely distant earthquakes will have a very low triggered fraction and can be used to approximate b_U. Note that this definition of the untriggered population may include many earthquakes that are triggered by other, unidentified local mainshocks. It has been proposed elsewhere that the fraction of locally triggered events catalog-wide is large and so essentially any group of earthquakes will contain aftershocks [*Marsan et. al.,* 2008]. However, for the purpose of this study we are asking if a group of identifiable, remotely triggered events has magnitude behavior that is distinct from other groups of earthquakes. This is a key question for both operational forecasting and physical understanding of the dynamic triggering process.

Data and Analysis Method

Event location, depth, origin time, and magnitude are extracted for the period 01 Jan 2009 to 01 Jan 2014. This period was chosen because of a California-wide change in the definition of M_L, implemented in 2008 for hypocenters cataloged by the Southern

California Seismic Network (SCSN, network code CI) and in January 2009 for seismicity within the Northern California Seismic Network (NCSN, network code NC) [*Hutton*, 2010; *Tormann et. al.*, 2010; *Uhrhammer et. al.*, 2011]. Data with network codes NC and CI were accessed from the Advanced National Seismic System (ANSS) Catalog (last accessed Jan. 2014, http://www.ncedc.org/). Events with depth greater than 30 km and magnitude less than M_C=1.8 are discarded to yield a complete and uniform catalog within the state of California vicinity (32 < Lat. < 42, -124 < Lon. < -114). Data from Nevada (NN code) is purposefully excluded from the ANSS search because of systematic differences in magnitude determination [*Uhrhammer et. al.*, 1996]. The *b*-value and 95% confidence level, generated via 1000 bootstrap resamplings, for the combined CI and NC seismicity is 0.86 ± 0.01.

In order to identify earthquake populations with strong triggering, we need to estimate the local peak ground velocity from a distant earthquake. We make this estimate by inverting a surface wave magnitude regression appropriate at both regional and teleseismic distances. Our target catalog is partitioned into ~1300 spatial nodes with accompanying seismicity within a 5 km radius (Figure 1). This grid scale encompasses approximately the same area as the 0.1°x0.1° grids selected in *van der Elst and Brodsky* [2010]. For each node, we loop through a global catalog of 'test triggers.' Events with magnitude M_W>5 from the ANSS catalog qualify for inclusion as a test trigger. Depths are limited to those shallower than 50 km because of their greater relative efficiency at generating surface waves. Additionally, each global test trigger must be at least 200 km from a local node. At the reference period of T=20 seconds,

$$M_S = \log_{10}(A_\mu) + \frac{1}{2} \cdot \log_{10}(\sin(\Delta)) + 0.0031 \cdot \Delta - \log_{10}(f_c) + 2.57 \tag{6}$$

where A_μ is the zero-to-peak amplitude in microns, Δ is the epicentral distance in degrees [*Russell*, 2006]. The parameter f_c corrects for the zero-phase third-order Butterworth filter applied to the data and is equal to $0.03 \cdot (\Delta^{-1/2})$. Since equation (6) is an empirically derived regression, we do not actually apply any filters to any seismic waveforms; we simply replace the M_S value in the equation with the M_W for the test trigger given in the catalog. Although M_S and M_W are not strictly the same quantity, the M_W scale has been calibrated to approximate the M_S scale for values less than $\sim M_W$=8 (the point where M_S begins to saturate) [*Kanamori*, 1977]. Finally, we estimate strain, ε, by assuming $\varepsilon = V/C_S$, where V is the particle velocity (approximately equal to $2 \cdot \pi \cdot f \cdot A$ [*Aki and Richards*, 2002], with A inverted from equation (6)) and C_S is the surface wave group velocity (3.5 x 10^9 μm/s for Rayleigh waves). Second order effects due to depth, rupture directivity, and radiation pattern are not captured by these regressions and can result in errors as high as 1 order of magnitude in extreme cases, but the global average curve will accurately predict the average strain of a large group of potential triggering events.

For a group of target areas that have experienced given amplitudes of shaking we can measure the inter-event time ratio, or R, as a proxy for measuring the fractional rate change [*van der Elst and Brodsky*, 2010]. The time ratio is defined as

$$R \equiv \frac{t_2}{t_1 + t_2} \tag{7}$$

where t_1 and t_2 are times to the first earthquakes before (with magnitude M_1) and after (with magnitude M_2) the arrival of seismic energy from some potential far-field trigger (Figure 2). In the absence of triggering the population of R-values will be distributed according to the standard uniform distribution with μ=0.5 and σ^2=1/12. In the presence of triggering, there will be a slight bias toward small values of t_2, leading to a larger proportion of small R-values and therefore a deflection of the mean value of R, $\bar{\boldsymbol{R}}$, to less than 0.5.

Prior work has shown that measurements of $\bar{\boldsymbol{R}}$ can be used to estimate rate changes induced by static stresses near a mainshock [*Felzer and Brodsky*, 2005] or changes in response to dynamic stresses like the passage of transient surface waves [*van der Elst and Brodsky*, 2010]. In particular,

$$\overline{R} = \frac{1}{\delta\lambda} \cdot [(\delta\lambda + 1) \cdot \ln(\delta\lambda + 1) - \delta\lambda] \tag{8}$$

where $\delta\lambda = (\lambda_2 - \lambda_1)/\lambda_1$, and λ_1 and λ_2 are the rates of seismicity before and after the arrival of the purported trigger [*van der Elst and Brodsky*, 2010, equation (2)]. For the purpose of utilizing equation (5), we need to measure the fraction of a dataset comprised of triggered earthquakes.

While the time period between 2009 and 2014 has homogeneous magnitude determination procedures, the data length (5 years) is less than ideal for generating a robust fractional rate change curve a la *van der Elst and Brodsky* [2010]. We remedy this situation by using an alternate, longer, time period to estimate fractional rate change from 1984 – 2014 (Figure 3).

Fractional rate change

Inverting for b_T from the mixing model equation (equation (5)) requires an estimate of the fraction of the data attributed to triggered earthquakes, or f_T. For a given source volume with a distribution of faults, we model the seismicity of the volume as a Poisson process with an average intensity parameter λ. Dynamic strains traveling through a source volume can activate faults and induce a step change in the intensity parameter from λ_1 to λ_2. For a stepwise homogenous Poisson process, we define the fractional rate change induced by some far-field trigger as

$$\delta\lambda = \frac{\lambda_2 - \lambda_1}{\lambda_1} \tag{11}$$

Over one pre-trigger recurrence interval (time $\tau = \lambda_1^{-1}$), the expected number of earthquakes in the post-trigger aftermath is $n_{after} = \delta\lambda + 1$ (the number expected in the recurrence interval prior to the test trigger is $n_{before} = \lambda_1 \cdot \lambda_1^{-1} = 1$). We can therefore define f_T as

$$f_T = \frac{n_T}{n_{tot}} = \frac{n_{tot} - n_U}{n_{tot}} = \frac{n_{after} - n_{before}}{n_{after}} = \frac{(\delta\lambda + 1) - 1}{\delta\lambda + 1} = \frac{\delta\lambda}{\delta\lambda + 1} \tag{12}$$

The mean of a sample of R-values from the longer catalog (Figure 3) is used to estimate $\delta\lambda$ (via equation (8)) and f_T (via equation (12)).

The finite length of an earthquake catalog introduces a bias in the calculation of R values. Unequal conditioning of t_1s and t_2s (Figure 2) can be introduced as the test trigger

time moves away from the middle of the local catalog. We remove this bias by truncating our local catalog to windows symmetric about the arrival time of each test trigger. Once f_T has been estimated for each group of earthquakes with similar values of dynamic strain, we then measure the composite *b*-value (b_{MIX}) and proceed to infer a range of values for b_T that is consistent with the data.

Sampling Biases and Results

Aftershock Shielding Effect

The final requirement to infer b_T is a measurement of b_U, the reference background seismicity parameter. We initially attempted to define b_U using events from the population of M_1 events. In that case, we supposed that the magnitude of the event immediately preceding the arrival of dynamic stress was an accurate representation of the steady-state distribution of magnitudes in a system unperturbed by far-field transient waves. However, we found that over the entire range of strain, the bias-corrected M_1 population shows a consistently higher *b*-value (corresponding to a lower mean magnitude) than its equivalent population of bias-corrected M_2 magnitudes (Figure 4). This is not an effect of finite time windowing, but rather stems from the clustering of earthquakes into aftershock sequences. We therefore call this the aftershock shielding effect. Figure 5 shows a schematic diagram demonstrating the origin of the systematic offset of magnitudes between the M_1s and M_2s. When a larger than average earthquake occurs, it tends to generate aftershocks. The time to the first earthquake in this aftershock sequence tends to be shorter than the time to the first earthquake that preceded the mainshock. Seismic waves from a distant earthquake are thus much less likely to fall

within the latter interval than the former. This means that a large magnitude local mainshock is systematically biased to be labeled an `$M_2$' versus an `M_1.' The large mainshock is shielded from being labeled an M_1 by its ensuing aftershocks.

Foreshock Shielding Effect

The presence of foreshocks induces a similar shielding effect. In Figure 3, the *b*-values of the M_2 data are systematically larger than the *b*-value of the overall catalog (~0.86). Since foreshock sequences follow an Inverse Omori Law, as far-field triggers approach the time of a local mainshock, they may fall within the rate increases (in an average sense) that precede the local mainshock.

ETAS Simulation

We can reproduce both of these shielding effects in an epidemic-type aftershock model (ETAS) [*Ogata*, 1998]. Following the procedure of Brodsky [2011], we produced a synthetic catalog with a b value of 1 and measured the magnitude distribution of the events prior and after randomly selected times. We found for 100 simulations that the M_1 *b*-value = 1.22±0.04 and the M_2 *b*-value = 1.0±0.03, with 1 standard deviation reported.

As discussed in Brodsky [2011], standard ETAS simulations have too few foreshocks (relative to aftershocks) compared to the observations. This disparity is due to either completeness problems or a physical propensity for foreshocks. The overabundance of foreshocks is an interesting issue in itself, however, here we are only concerned with its effect on the sampling of magnitudes. Therefore, since the standard ETAS simulation using standard parameters only reproduced the aftershock shielding and did not explain the deviation of the M_1s in the observations, we performed an additional set of modified ETAS simulations that mimic the large fraction of foreshocks. To

illustrate the foreshock abundance of real catalogs, a fraction of the aftershocks were randomly assigned to occur as foreshocks, i.e., the sign of the time from the mainshock is reversed. We emphasize that this adaptation of the ETAS model is employed simply as a tool to investigate the effects of foreshocks on selection of earthquakes. If 25% of the aftershocks are turned into foreshocks, the observed aftershock to foreshock ratio was close to the catalog values (~2) and the observed M_1 *b*-value = 1.19±0.03 (1 std.) and the M_2 *b*-value = 1.10±0.04 (1 std.), which offset approximately .1 and .2 units from the catalog wide *b* value. These offsets from the catalog wide value match in a bulk sense the offsets observed in actual data (Figure 4). We conclude from this exercise that the offsets between the M_1 and M_2 populations can be explained as a natural consequence of the effect of earthquake foreshock and aftershock sequences on selecting earthquakes. No more elaborate hypothesis about triggered magnitudes is necessary.

Because of the sampling biases mentioned above, the most meaningful reference magnitudes must also come from the M_2 data set. We take the values of M_2 corresponding to the lowest fractional rate changes (*i.e.*, $\varepsilon \sim 10^{-9}$) to represent the parameter b_U, equal to 1.02 (Figure 4). Next we apply the mixing model to b_{MIX} data to extract b_T from the 3 observable variables: b_{MIX}, b_U, and f_T. Figure 6 shows the results of the b_T inversion for the combined catalog. At face value, these observations suggest that *b*-values of data with high percentage of triggered earthquakes are on average larger (*i.e.*, smaller magnitude) than the *b*-values of untriggered or spontaneous seismicity. Error bars are derived from 5000 bootstrap resamplings (sampling with replacement) of the M_2 values in each amplitude bin [*Efron and Tibshirani*, 1994]. The errors associated with these

measurements indicate, however, that these differences are insignificant and cannot be distinguished from background seismicity.

Implications

Our results indicate there are no discernible differences between the magnitude distributions of data sets that likely contain a high proportion of triggered events, versus data sets that do not contain high proportions of triggered events. The observed composite *b*-values (b_{MIX}, black curve in Figure 4) show no significant variation with respect to calculated peak dynamic strains (Figure 4). The small variations that do exist do not show a monotonic trend with the fraction of likely triggered events in the population, meaning that this conclusion is not likely to change with increased statistical resolution. Inverting for b_T directly using a mixing model does not alter these conclusions (Figure 6).

These interpretations are significantly different than that of Parsons and Velasco [2011] who suggested that dynamically triggered earthquakes are preferentially small. These studies differ in fundamental ways. For instance, the statistical treatment here includes greater than 400 examples of potential triggers for each data set, including some very weak triggers, and deals explicitly with the fact that any observed group of earthquakes is a mixture of triggered and untriggered events via our mixing model. The previous work had 205 examples of very strong triggering. Secondly, the *R*-statistic uses an optimized, adaptive time window to measure rate changes and therefore is inherently more sensitive than the counting method of Parsons and Velasco. Finally, we focus on small earthquakes as diagnostic of the magnitude distribution; this contrasts with the

approach of Parsons and Velasco where only $5 < M_W < 7$ events are examined. The advantage of this paper's approach is that larger numbers ensure statistical robustness since larger magnitude earthquakes are intrinsically rare and may not be expected to be observed during a short time interval.

It has recently been argued that the 2012 M_W8.7 strike-slip earthquake off the coast of Sumatra remotely triggered large (M_W>5.0) earthquakes along the circum-Pacific boundary in the days following the passage of mainshock surface waves [*Pollitz et. el.*, 2012]. If larger magnitude earthquakes have distinct physical nucleation mechanisms our approach has no bearing on them. Thus far, there is little direct evidence of a distinct process controlling the magnitude of large earthquakes, therefore a separate process governing large earthquakes could be a relatively unlikely possibility, but one that must remain open nonetheless.

Conclusions

We find that the statistical evidence for fundamentally different underlying distributions between triggered and untriggered earthquakes is weak. This strongly supports the idea that the magnitudes of triggered and untriggered earthquakes are randomly drawn from a single parameter GR distribution, at least for moderate magnitudes. Therefore, remotely triggered earthquakes are likely to be as large as any other group of seismicity. However, since the total number of triggered events is small, the probability of observing a remotely triggered large earthquake is accordingly small. In summary, we have opted for large numbers in our statistical treatment and arrived at

conclusions distinct from prior efforts. This suggests that the question of the magnitude distribution of dynamically triggered events is still an open problem.

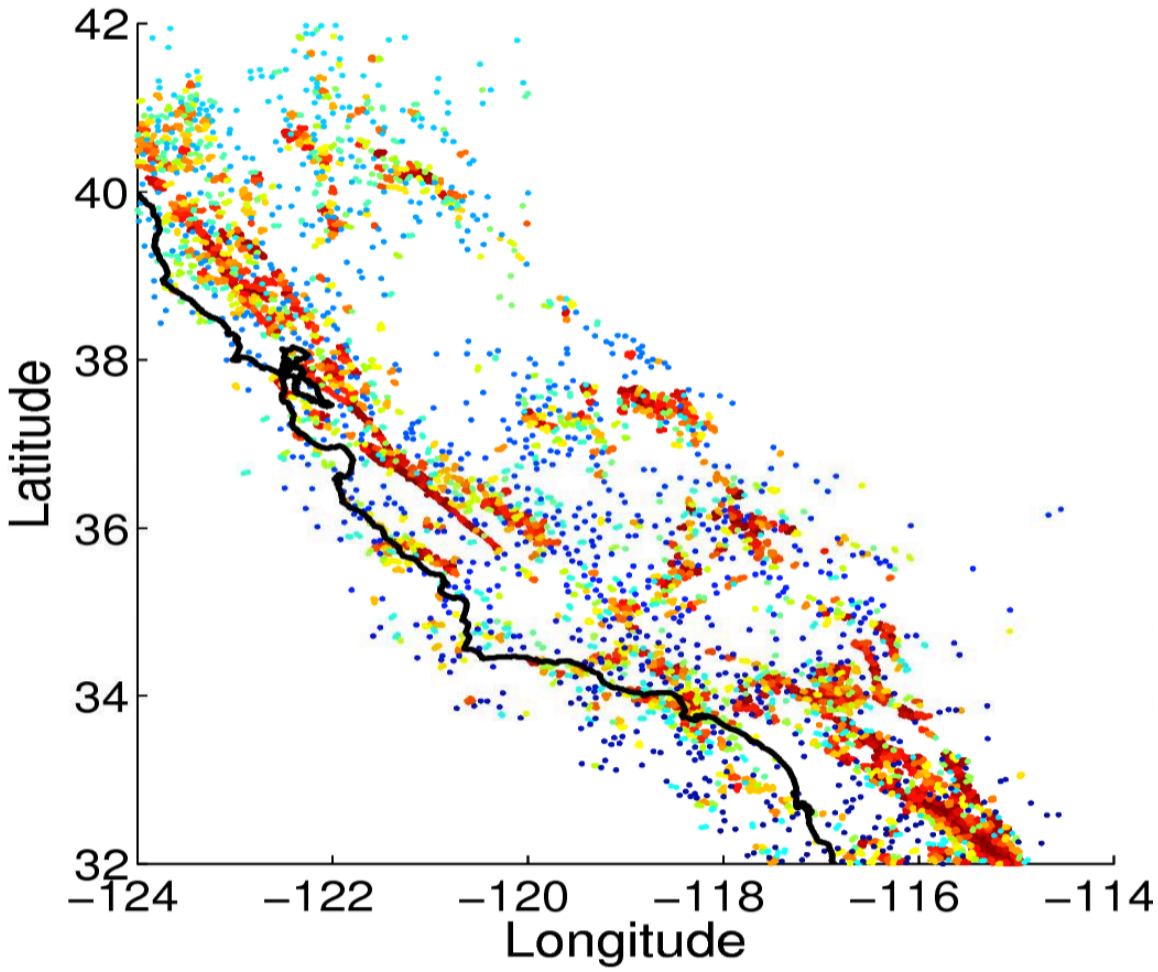

Figure 1: 1298 nodes with seismicity greater than magnitude 1.8 and occurring after 01 Jan 2009. Hues are scaled to data density. Seismicity outside of California and with less than 2 data points within a 5 km radius of the spatial node are not analyzed. Thick black line is the coast.

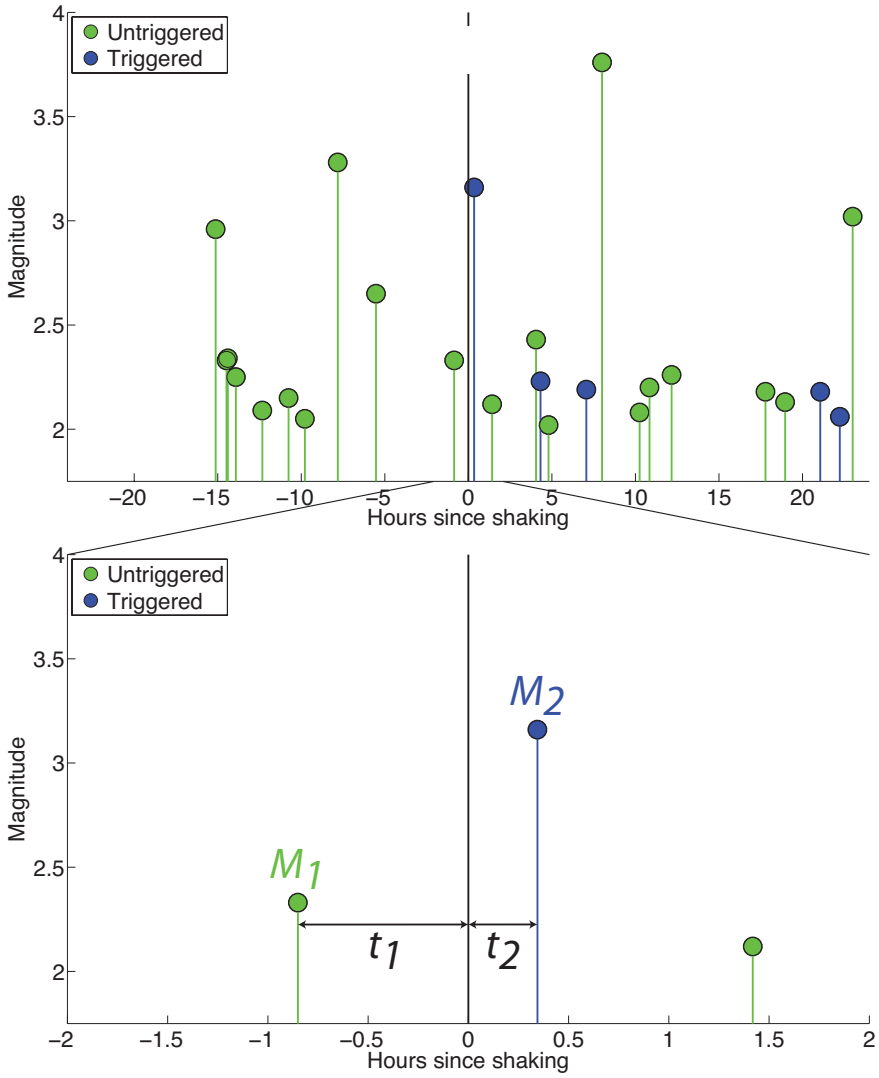

Figure 2: Schematic cartoon of hypothetical synthetic data from a single grid node, demonstrating the procedure for measuring *R* values. The vertical black dashed line is the approximate arrival time of seismic energy from one far-field event, i.e., 'test trigger'. In this hypothetical example, a symmetric window of ±1 day (24 hours) is imposed. In practice, we impose a symmetric window of ±2 years.

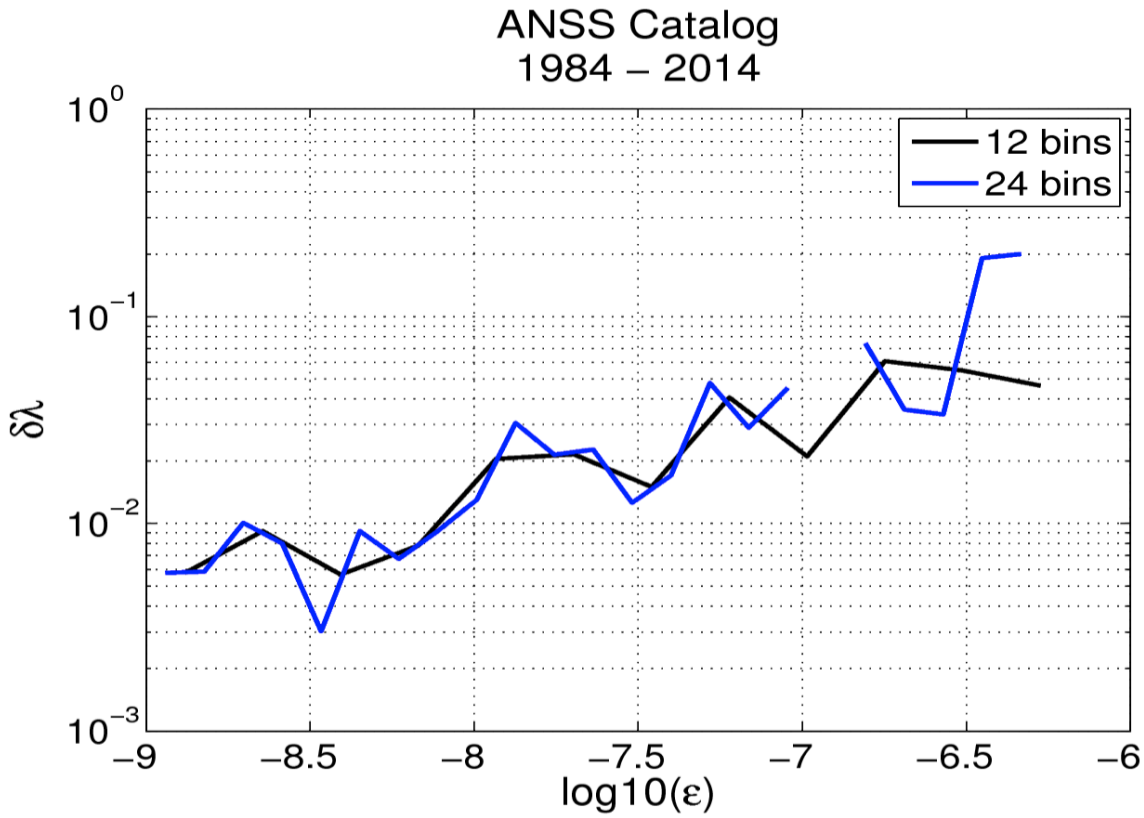

Figure 3: Triggering intensity (fractional rate change, $\delta\lambda$) for the ANSS California seismicity between 1984 – 2014, with magnitude of completeness 2.1. 2 year symmetric windows about each test trigger were applied, and an R ratio determined. For narrow amplitude bins, the mean R ratio was converted to a fractional rate change via Equation 8.

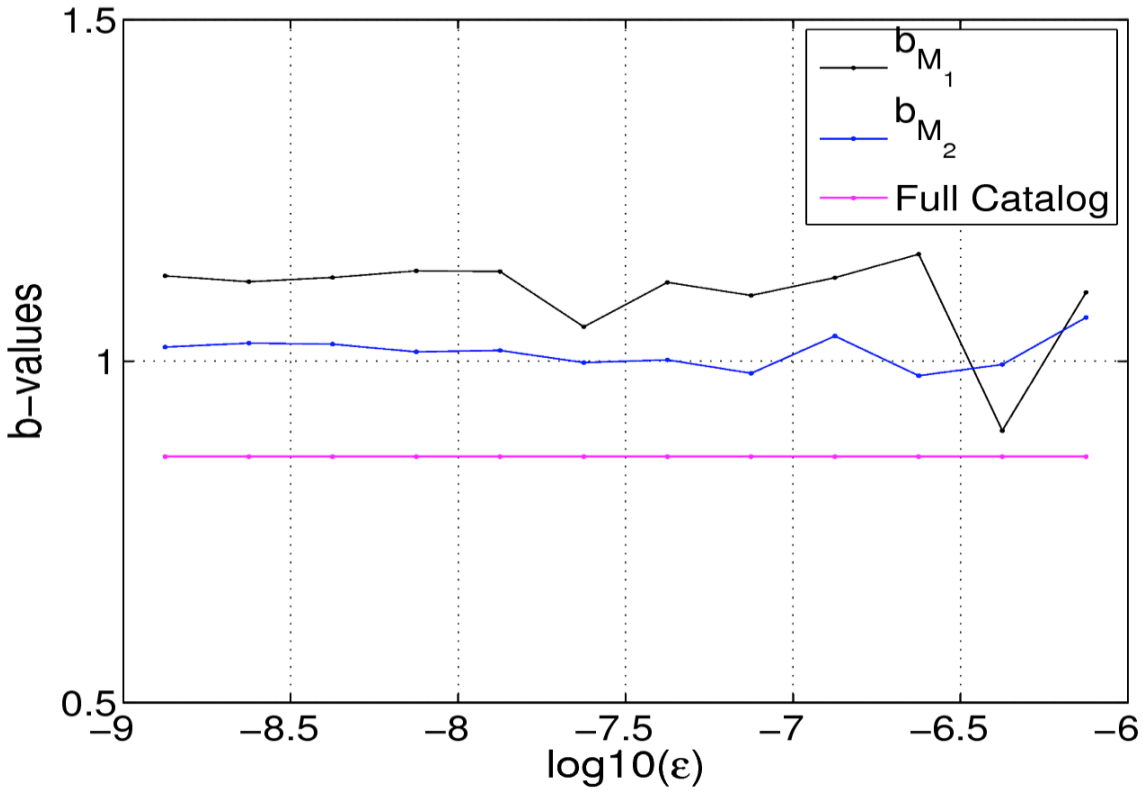

Figure 4: *b*-values for the M_1 and M_2 populations of data as a function of peak dynamic strain. Both curves show *b*-values higher than the catalog-wide value (magenta curve). The persistent static offset between the two curves is due to the aftershock shielding effect (see text for details).

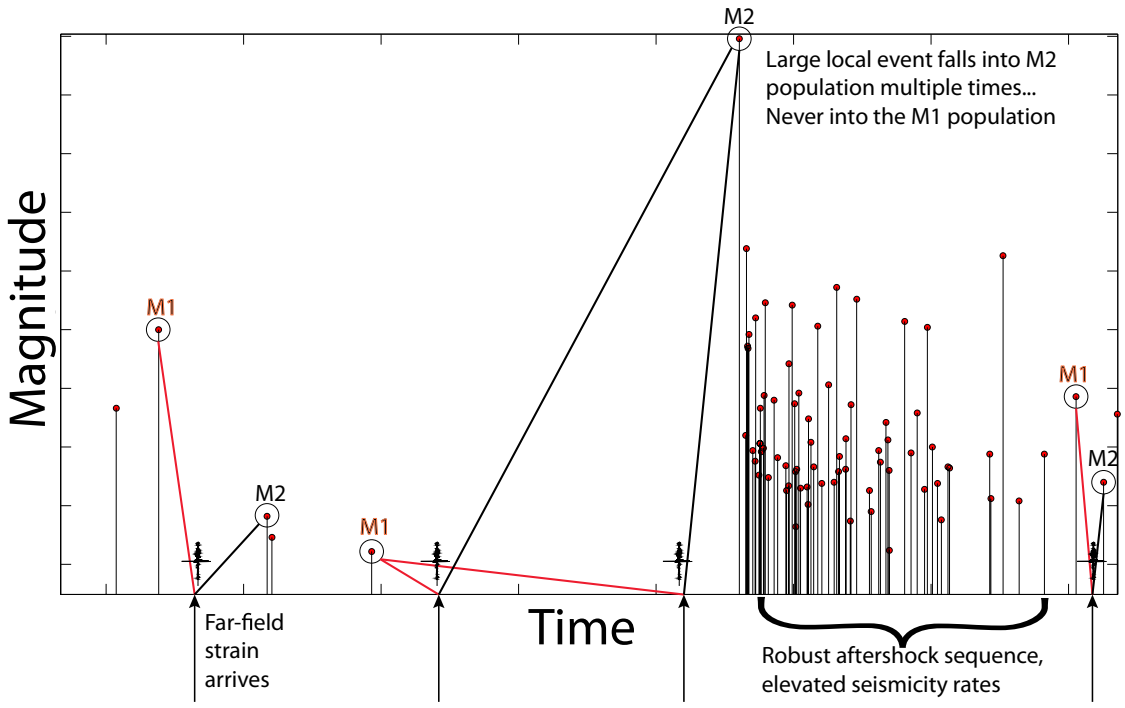

Figure 5: Schematic diagram for the origin of the systematic offset of magnitudes between the M_1s and M_2s. Teleseismic waves arriving in our target catalog are represented by black arrows. For each far field event, a unique R-ratio is calculated and an M_1 and M_2 within the local catalog are identified. When a local mainshock occurs, the time to the next event is, on average, substantially reduced as aftershocks tend to cluster in time and space. It is therefore unlikely that teleseismic surface waves will arrive in the time interval between the local mainshock and its first local aftershock. Therefore, the large local mainshocks in a target catalog are rarely designated as M_1s, and almost always designated M_2s. Hence, the systematic offset in magnitudes between the two datasets. We call this the aftershock shielding effect.

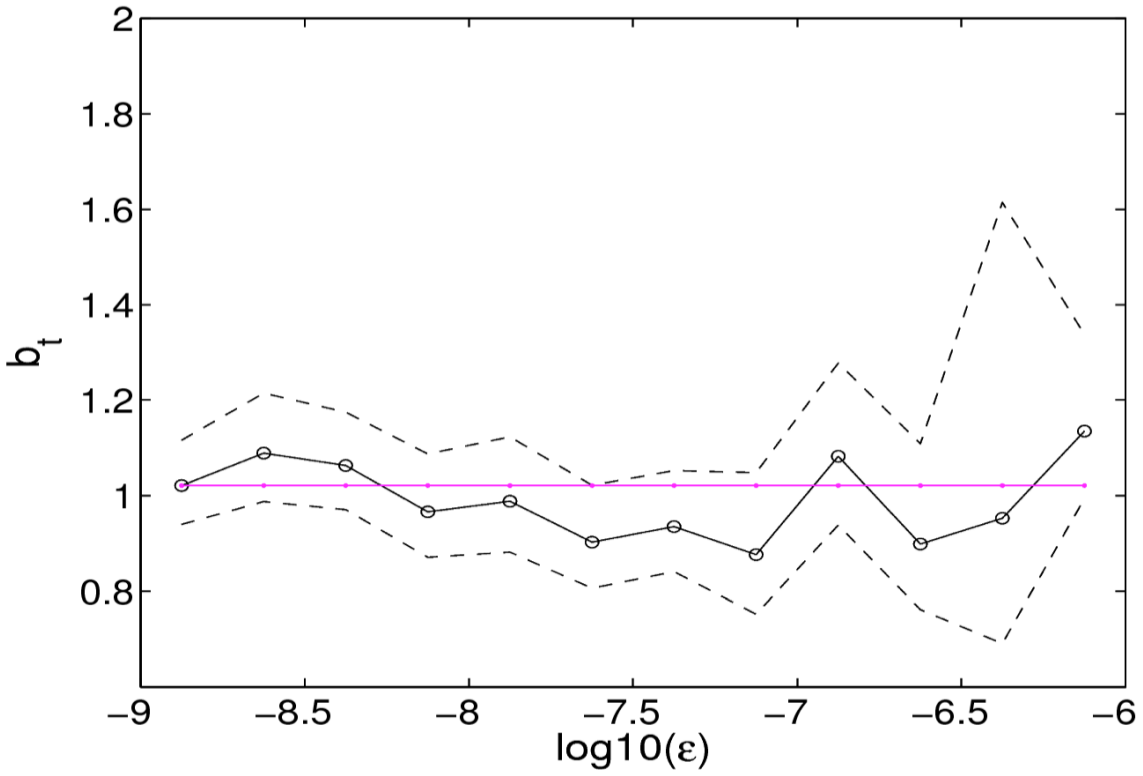

Figure 6: b_T as inverted from Eq. (5) for combined catalog. The horizontal line corresponds to an estimate of b_U based on data from the strain measurements smaller than $1x10^{-9}$. Error bars derived from 5,000 bootstraps indicate the triggered *b*-values *(b_T)* are insignificantly different from our reference b_U.

References

Aki, K. (1965), Maximum likelihood estimate of b in the formula log N = a − bM and its confidence limits, *Bull. Earthquake Res. Inst. Tokyo Univ.*, 43, 237–239.

Aki, K., and P. G. Richards (2002), Quantitative Seismology, 2nd ed., 700 pp., *Univ. Sci. Books*, Sausalito, Calif.

Brodsky, E. E. (2006), Long-range triggered earthquakes that continue after the wave train passes, *Geophys. Res. Lett.*, 33, L15313, doi:10.1029/2006GL026605.

Brodsky, E. E. (2011), The spatial density of foreshocks, *Geophys. Res. Lett.*, *38*, L10305, doi:10.1029/2011GL047253.

Efron, B and R.J. Tibshirani (1994), An Introduction to the Bootstrap, 436 pp., *Monographs on Statistics and Applied Probability*, CRC Press, Boca Raton, FL.

Felzer, K. R., and E. E. Brodsky (2005), Testing the stress shadow hypothesis, *J.Geophys. Res.*, 110, B05S09, doi:10.1029/2004JB003277.

Felzer, K. R., T. W. Becker, R. E. Abercrombie, G. Ekstrom, and J. R. Rice (2002), Triggering of the 1999 MW 7.1 Hector Mine earthquake by aftershocks of the 1992 MW 7.3 Landers earthquake, *J. Geophys. Res.*, 107 (B9), 2190, doi:10.1029/2001JB000911.

Felzer, K. R., R. E. Abercrombie, and G. Ekstrom (2004), A common origin for aftershocks, foreshocks, and multiplets, *Bull. Seismol. Soc. Am.*, 94, 88–98.

Frohlich, C., and S. D. Davis (1993), Teleseismic b values; or much ado about 1.0, *J. Geophys. Res.*, 98 (B1), 631–644, doi:10.1029/92JB01891.

Gomberg, J., and D. Agnew (1996), The accuracy of seismic estimates of dynamic strains: An evaluation using strainmeter and seismometer data from Pinon Flat

Observatory, California, *Bull. Seismol. Soc. Am.*, 86, 212–220.

Gutenberg, B., and C. F. Richter (1944), Frequency of earthquakes in California, *Bull. Seismol. Soc. Am.*, 4, 185–188.

Hill, D. P., et al. (1993), Seismicity remotely triggered by the magnitude 7.3 Landers, California, earthquake, *Science*, 260(5114), 1617–1623.

Hutton, K., J. Woessner, and E. Hauksson (2010), Earthquake monitoring in Southern California for seventy-seven years (1932 - 2008), *Bull. Seismol. Soc. Am., 100, 423 – 446*

Holschneider, M., G. Zoller, and S. Hainzl (2011) Estimation of the maximum possible magnitude in the framework of a doubly-truncated Gutenberg-Richter model, *Bull. Seismol. Soc. Am., 101, 1649 – 1659*

Ishimoto, M., and K. Iida (1939), Observations of earthquakes registered with the microseismograph constructed recently, *Bull. Earthquake Res. Inst. Univ. Tokyo*, 17, 443–478.

Kanamori, H. (1977), The energy release in great earthquakes, *J. Geophys. Res.*, 82, 2981-2987

Kijko, A. and A. Smit (2012), Extension of the Aki-Utsu *b*-value estimator for incomplete catalogs, *Bull. Seismol. Soc. Am.*, *102*, 1283–1287.

King, G. C. P., R. S. Stein, and J. Lin (1994), Static stress changes and the triggering of earthquakes, *Bull. Seismol. Soc. Am.*, 84, 935–953.

Marsan, D., and O. Lengliné (2008), Extending earthquakes' reach through cascading, *Science*, 319, 1076–1079.

Ogata, Y. (1998), Space−time point−process models for earthquake occurrences, *Ann. Inst. Stat. Math.*, *50* (2), 379–402.

Parsons, T., and A. A. Velasco (2011), Absence of remotely triggered large earthquakes beyond the mainshock region, *Nature Geoscience*, 4, 321–316, doi:10.1038/ngeo1110.

Parsons, T., J. O. Kaven, A. A. Velasco, and H. Gonzalez-Huizar (2012), Unraveling the apparent magnitude threshold of remote earthquake triggering using full wavefield surface wave simulation, *Geochem. Geophys. Geosyst.*, 13, Q06016, doi:10.1029/2012GC004164.

Pollitz, F. F., R. S. Stein, *and* R. Burgmann *(*2012*),* The 11 April 2012 M = 8.6 East Indian Ocean earthquake triggered large aftershocks worldwide*, Nature,* 490*,* 250–253*, doi:*10.1038/nature11504.

Russell, D. R. (2006), Development of a time-domain variable-period surface-wave magnitude measurement procedure for application at regional and teleseismic distances, part I: theory, *Bull. Seismol. Soc. Am.*, *96*, 665–677.

Shelly, D. R., Z. Peng, D. P. Hill, and C. Aiken (2011), Triggered creep as a possible mechanism for delayed dynamic triggering of tremor and earthquakes, *Nature Geoscience*, *4*, 384–388

Schorlemmer, D., S. Weimer, and W. Wyss *(*2005*),* Variations in earthquake-size distribution across different stress regimes *, Nature,* 437*,* 539–542 doi:10.1038/nature04094

van der Elst, N. J., and E. E. Brodsky (2010), Connecting near-field and far-field

earthquake triggering to dynamic strain, *J. Geophys. Res.*, 115, B07311, doi:10.1029/2009JB006681.

van der Elst, N. J., E. E. Brodsky, and T. Lay (2013)Precursory remote triggering is absent near the epicenters of great earthquakes, *Bull. Seismol. Soc. Am., in press*

Velasco, A. A., S. Hernandez, T. Parsons, and K. Pankow (2008), Global ubiquity of dynamic earthquake triggering, *Nature Geoscience*, 1, 375–379.

Uhrhammer, R. A., S. J. Loper, and B. Romanowicz (1996), Determination of Local Magnitude Using BDSN Broadband Records, *Bull. Seismol. Soc. Am.*, *86*, 1314–1330.

Uhrhammer, R. A., M. Hellweg, K. Hutton, P. Lombard, A. W. Walters, E. Hauksson, and D. Oppenheimer (2011), California Integrated Seismic Network (CISN) Local Magnitude Determination in California and Vicinity, *Bull. Seismol. Soc. Am.*, *101*, 2685–2693.

Utsu, T. (1965). A method for determining the value of b in the formula log n = a - bM showing the magnitude-frequency relation for earthquakes, *Geophys. Bull. Hokkaido Univ.*, 13, 99–103 (in Japanese with English summary).